HAFIZ MUHAMMAD AWAIS RASHID[1], MUHAMMAD GHAZZALI[1],
UMER WAQAS[1]*, ADNAN ANWAR MALIK[2],
MUHAMMAD ZUBAIR ABUBAKAR[3]

ARTIFICIAL INTELLIGENCE-BASED MODELING FOR THE ESTIMATION OF Q-FACTOR AND ELASTIC YOUNG'S MODULUS OF SANDSTONES DETERIORATED BY A WETTING-DRYING CYCLIC PROCESS

In this study, a series of destructive and non-destructive tests were performed on sandstone samples subjected to wetting-drying cycles. A total of 25 Wet-Dry cycles were provided to investigate any significant change in the engineering properties of sandstones in terms of their porosity, permeability, water absorption, density, Q-factor, elastic modulus (E), and unconfined compressive strength (UCS). The overall reduction in the values of density, E, Q-factor, and UCS was noted as 3-4%, 42-71%, 34-62%, and 26-70% respectively. Whereas, the overall appreciation in the values of porosity, permeability, and water absorption was recorded as 24-50%, 31-64%, and 25-50% respectively. The bivariate analysis showed that the physical parameters had a strong relationship with one another and their Pearson's correlation value (R) ranged from 0.87-0.99. In prediction modeling, Q-factor and E were regressed with the contemplated physical properties. The linear regression models did not provide satisfactory results due to their multicollinearity problem. Their VIF (variance inflation factor) value was found much greater than the threshold limit of 10. To overcome this problem, the cascade-forward neural network technique was used to develop significant prediction models. In the case of a neural network modeling, the goodness of fit between estimated and predicted values of the Q-factor ($R^2 = 0.86$) and E ($R^2 = 0.91$) was found much better than those calculated for the Q-factor ($R^2 = 0.30$) and E ($R^2 = 0.36$) in the regression analysis.

**Keywords:** Wetting and Drying Cycles, Rock Permeability, Dynamic Elastic Young's Modulus, Q-factor, UCS

---

[1] UNIVERSITY OF ENGINEERING AND TECHNOLOGY, DEPARTMENT OF GEOLOGICAL ENGINEERING, LAHORE, PAKISTAN
[2] SAITAMA UNIVERSITY, DEPARTMENT OF CIVIL AND ENVIRONMENTAL ENGINEERING, JAPAN
[3] UNIVERSITY OF ENGINEERING AND TECHNOLOGY, DEAN FACULTY OF EARTH SCIENCES AND ENGINEERING, LAHORE, PAKISTAN

* Corresponding author: umerwaqas@uet.edu.pk
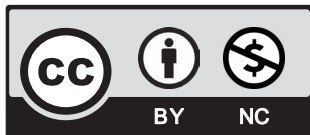
1. Introduction

The degradation of rocks is highly associated with water; and in rock engineering applications (ie tunneling and mining etc.), the rock mass is found in wet conditions. Significant changes in the groundwater level, humidity, and precipitation can cause periodic wetting and drying (W-D) in rocks which may accelerate the weathering processes. As a result karst collapse, landslides, pillar degradation in mines, and degradation of dam foundations may occur. Cyclic wetting and drying may also have a significant effect on the rock's dynamic properties. Thus, it is important to investigate the physico-dynamic characteristics of rocks subjected to the cyclic W-D process.

Water is one of the most important weathering agents that adversely affect the geomechanical characteristics of rocks. It not only weakens the rock mass but also deteriorates the rock fabric. The engineering properties of rocks mainly depend on their origin, mineral composition, texture, and rock fabric. After interaction with water, rocks get weakened because of the removal of cementing material between the grains and alteration in mineral composition. The change in mineral composition is the result of chemical reactions with the naturally occurring slightly acidic or basic water. Małkowski et al. [48] found that the geomechanical properties of rocks are the function of their mineral composition and they get varied at different saturation levels. Similarly, Vàsàrhelyi and Vàn [49] observed that the physico-mechanical properties of sedimentary rocks such as sandstone depreciate with the increase in the degree of saturation. They also noticed that in some cases with 1% water saturation rock strength decreases remarkably.

Different experimental studies on sandstones have shown that in saturated conditions, sandstones suffer a significant loss in strength [1]. In the case of clay-bearing rocks, saturation-induced stiffness, and strength reduction is up to 80% [4]. Gökceoğlu et al. [6] investigated various factors that may affect the slake durability index of clay-bearing rocks and found that the type and amount of clay minerals are the main factors affecting the slake durability index. However, if the main constituent of the sandstone is quartz with no clay minerals, there was no significant effect of saturation on the strength of the sandstones. The presence of clay minerals decreases the strength of sandstones mainly due to the dissolution of clay minerals in water during wetting cycles [6]. However, the decrease in strength was also found to be dependent on the clay content and composition of clay minerals. A large clay content contributes to a weaker quartz-clay framework that results in a reduction in strength on wetting. Correspondingly, an increase in chlorite content was found to contribute more to the reduction of strength compared to montmorillonite and illite [8].

Deterioration is caused not only by wetting and drying but also by freeze and thaw weathering, insolation, thermal shock, and other environmental factors that play a significant role in strength reduction. In the recent past, the effects of W-D cycles on the physical characteristics of rocks have been studied by several researchers [9]. The weakening in rocks was evaluated by examining the changes in the physico-mechanical characteristics of the rocks. These properties mainly include water absorption, porosity, bulk density, and P-wave velocity. The studies showed that an increasing number of W-D cycles considerably alter the above-mentioned rock characteristics.

Deng et al. [13] showed that alternating W-D cycles play a significant role in affecting the physical and mechanical properties of sandstone. The investigations regarding mechanical properties of the rocks under W-D cycles have been mainly focused on uniaxial compressive strength, tensile strength, shear strength, and fracture toughness [14] [12]. The results of the studies showed that the mechanical properties and degree of deterioration vary greatly due to cyclic wetting-drying treatments.

The change in these properties due to the strength and weathering conditions of building stones was of interest to petrologists for many years of investigation. Studies on weathering of sandstone are related to morphological elements, process operation, change in environmental conditions that control these processes, and the respective materials on which the process operates [18]. Many studies have highlighted the significance of the porosity of rocks and the distribution of the pore size as a determinant of the weathering of rocks [19]. Matrix mineralogy and the distribution of the pore radius, as well as the degree of cementation, are the main factors that determine what effect does partial water saturation has on the strength of rocks [21].

Most of the studies mentioned above were focused on the static mechanical properties of rocks. Limited research was carried out to study the effect of W-D cycles on the dynamic characteristics. Usually, in the field of rock engineering, the rocks are fractured dynamically e.g during impact, blasting, rock bursting, and seismic events. Therefore, it is quite important to investigate the change in physical as well as dynamic properties of the rocks under cyclic wetting and drying to assess the stability, safety, and serviceability of rock structures.

The recommended practice for the determination of rock engineering properties in the laboratory or field is a time taking job [22]. That needs highly calibrated instruments, good expertise, and precision. Sometimes, rock engineering properties cannot be determined through standard practice because of some impeding factors such as time, budget, conditions, limited supply of samples, unavailability of required instruments, etc. [23]. In such circumstances, researchers have favored using empirical relationships to find rock engineering properties. Several empirical relationships have been made between different rock strength parameters using multivariate statistics, supervised or unsupervised machine learning, neural network, fuzzy logic, etc. [22]. In the literature, no meaningful predictive relationships were found between the physico-dynamic properties of the sedimentary rocks damaged under wetting-drying cycles.

Prediction modeling through multivariate statistics and the artificial neural network has widely been accepted in rock mechanics and related studies. In multiple linear regression modeling, a dependent variable is regressed with two or more predictors to get the best fit-line [28]. This linear relationship between parameters may adversely be affected by the multicollinearity problem. If variables are highly dependent on one another the multicollinearity arises that may lead to overfitting of the model [29]. To control this problem, the variance inflation factor (i.e. overall model variance to a single variable variance) is calculated and its value must be less than 10 [25]. Apart from multivariate statistics, the artificial neural network can develop more reasonable predictive models than multivariate statistics. The neural network model works on human intelligence and can effectively solve artificial intelligence problems [29]. It receives input values as signals, assigns weights, and generates output much closer to the target values. The learning-training process and use of nonlinear activation function produce favorable outcomes. Researchers have proposed to use a neural network in prediction modeling because it is an adaptive process that adjusts the sudden changes in the provided values to get an optimal solution [28].

This study aims to anticipate the dynamic-physical behavior of selected sandstones subjected to wetting-drying cycles in terms of their density, porosity, permeability, water absorption, quality factor, and elastic modulus. Furthermore, it focuses on the development of the predictive relationships between dynamic-physical parameters of damaged sandstones under the wetting-drying cyclic effect using multiple regression and backpropagation cascade-forward neural network. The outcomes of this research work can be used as references in the stability analysis of rocks as a construction material, geotechnical site investigation, and subsurface modeling.
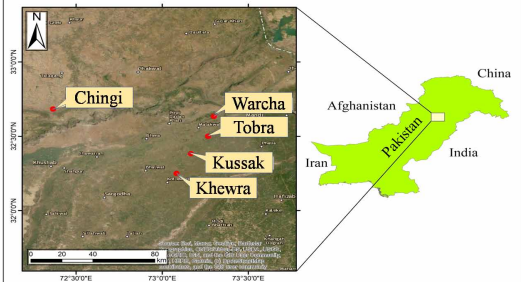
2. Field Visit and Sample Collection

The sandstone samples for this study were collected from the selected geological formations of the Salt Range area of Pakistan. The collected samples were intact without any noticeable imperfections and discontinuities. The size of each collected sample was in the range of 1.5 to 2 cubic feet which was sufficient to extract at least five cores of the required size for subsequent testing. The collected samples belonged to different geological formations namely Khewra, Kussak, Tobra, Warcha, and Chingi formations.

Khewra sandstone is extensively exposed in eastern flank area of the Salt Range, Pakistan. Khewra Sandstone is famous for dozens of primary geological features such as ripple marks, crossbedding, flame structure, mud cracks, etc. It is found as reddish-brown to yellowish-brown, fine to medium grain sandstone [30]. The sandstone of Kussak formation is mica rich and glauconitic in nature [32]. It is mainly composed of fine to medium grained particles and resting above the Khewra formation. Tobra formation is well exposed in the upper succession of the eastern flank of the Salt Range. It is dirty white to light grey coloured, medium to coarse grained sandstone. Warcha sandstone is pinkish-red to yellowish-red coloured, medium to coarse grained with interbedded shale and conglomerate. Grey coloured Chingi sandstone is in quartz, lithic fragments, and made of fine to medium-grained particles [33]. The selected geological formations and their respective geological age is described in Table 1.

TABLE 1

Selected sandstone samples of the various geological formations

Geological Formation	Geological Age	Location Map
Chnigi Formation	Miocene	
Warcha Formation	Permian	
Tobra Formation	Permian	
Kussak Formation	Cambrian	
Khewra Formation	Cambrian	

3. Methodology

3.1. Preparation of rock samples for testing

Standard NX size (54 mm diameter) cores were prepared by using a core cutting machine with a diamond drill bit following the recommended procedures of the International Society for Rock Mechanics [34]. The collected rock samples were assumed to have undergone a zero W-D cycle. In this study, a single W-D cycle was divided into two stages. The first stage consists of sample saturation from its dry state whereas the second stage deals with the drying of sample from the saturated state. The dry samples were fully saturated at laboratory temperature by fol-

lowing the progressive saturation technique developed by the US Army Corps of Engineers [35]. A sample was considered completely saturated when there was no further increase in the mass of the sample after it was left submerged in water for 12 hours. It was observed that complete saturation of a sample needed at least 48 hours. After saturation, the samples were oven-dried at 60°C for 24 hours. In this study, a total number of 25 W-D cycles were applied to each specimen. The physico-dynamic properties of the specimens were measured each 5 cycles.

3.2. Density, water absorption, and porosity measurement

Kurt-Karakus et al. [36] discussed a variety of methods to determine the density (ρ), porosity (Φ), and related properties of rocks. Among these "saturation and caliper method" and "saturation and buoyancy method" was the most frequently utilized techniques. In this research, the density and porosity tests were performed by employing the saturation and capillary technique [37]. The water absorption of the rock specimens was measured by the mass variation in a single wetting-drying cycle using the following formula:

$$W = \frac{(m_w - m_d)}{m_d} \times 100\%$$ (1)

where W (%) is the specimen water content, m_w (g), and m_d (g) are the wet and dry masses of the specimen, respectively.

3.3. Permeability (K)

A constant head rock permeability apparatus manufactured by the MATEST, Italy (Oil-Water Constant Pressure System for Permeability Test; model no. A144) was employed in this study to measure the permeability of rock specimens. The apparatus consisted of a Hoek cell, upper and lower spacers, a pressure controller, a pump, and a burette. The rock samples with a typical diameter (D) of 5.4 cm (cross-sectional area, A = 22.90 cm^2) and length (L) of 8.0 mm were prepared for this test. Permeability of rock samples was measured after every five W-D cycles using the following procedure.

Initially, the sample was inserted into Hoek's cell between upper and lower spacers. The inflow and outflow tubes were connected to the bottom and top of the cell. The inflow pipe was connected to the pressure controller and the outflow pipe was connected to a burette. Before applying confining pressure, water was permeated through the apparatus to remove air bubbles from inflow and outflow lines. A confining pressure of 1 MPa was then applied across the jacket to prevent sidewall leakage. The pressure head (P) was increased in a stepwise fashion (i.e.,200, 400, and 600 kPa) using a pressure controller, and the amount of effluent collected over some time *i.e.* flow (Q) was measured. A minimum of three measurements of flow (Q) was recorded against each pressure head (P) and the value of permeability (K) was calculated using the following formula (Eq. 2):

$$K = \frac{Q.L}{P.A}$$ (2)

where K – Permeability (cm/sec), Q – Flow (cc/sec), L – Sample length (cm), P – Pressure head (psi), A = Cross-sectional area of the sample (cm^2)

3.4. Elastic Young's Modulus (*E*)

Erudite Resonance Frequency Meter was used to estimate dynamic elastic Young's modulus of the rock specimens. The device consists of a control panel, a vibrator, and a receiver. The apparatus can provide a loading frequency from 1 kHz to 100 kHz. Kramer [38] reported that the determination of dynamic properties of rock material at higher loading frequency induces low strain. The tests were performed following [39]. The samples were tested at a recommended frequency of 6 kHz which is an extreme frequency for circular samples at longitudinal mode at the lowest output voltage (0.01V). To perform the test, the samples were clamped between the vibrator and receiver of the apparatus. It was assured that both tips were in contact with the rock sample. A frequency of 6 kHz was set as recommended in the standard. The test was run, and output values were recorded. Young's modulus was then calculated using the following formula (Eq. 3).

$$E = 519.14 \left(\frac{L}{D^2} \right) M \times \left(Fr^2 \right) \tag{3}$$

where L is the length of the sample (m), D is the diameter of the sample (m), M is the mass of the sample (kg), and Fr (kHz) is the resonance frequency.

3.5. Quality Factor (Q-factor)

To determine Q-factor Erudite Resonance Frequency Meter was employed. The Q-factor is a dimensionless parameter that describes the quality of the tested rock sample. It is an indirect way to discern the degree of compactness or looseness of rock samples [50]. It is the ratio of resonance frequency to the bandwidth. The bandwidth is the difference between the cut-off frequencies. Mathematically, it can be expressed as follows:

$$\text{Q-factor} = \frac{F_r}{F_h - F_l} \tag{4}$$

where: F_r is the resonance frequency, F_h is the increase in frequency above resonance, and F_l is the decrease in frequency below resonance.

3.6. Uniaxial Compressive Strength

The uniaxial compressive strength test was performed on the rock specimens at the 0th and 25th W-D cycles by following [40]. The samples were tested with a 200-ton Shimadzu Universal Testing Machine (UTM).

3.7. Petrographic Analysis of Rock Samples

Thin sections of tested rock samples were prepared to study the change in the mineralogical composition of the tested samples due to W-D cycles. Equivalent quartz content (EQC) of rock

samples was determined by utilizing the Rosiwal mineral abrasiveness ratio and computed by adopting the following equation (Eq. (4)) given by [41].

$$EQC = \sum V_i \times R_i \qquad (5)$$

where; EQC – mineral content stated in terms of quartz hardness using Rosiwal's hardness scale (in vol.%), V – quantity of mineral i (%), R – Rosiwal hardness of mineral i, n – total number of minerals.

3.8. Multivariate Statistics and Artificial Neural Network

In this study, two statistical techniques: multiple linear regression (MLR) modeling and backpropagation cascade-forward neural network (CFNN) were used for the predictive modeling of dynamic-physical parameters of cyclic wetting-drying treated sandstones. The MLR modeling was performed on the experimentally acquired dataset using the SPSS software package (version 26) to obtain a best-fitted regression model having minimum values of residuals or errors. Whereas, prediction modeling through the neural network was conducted using the MATLAB (version 2015) codes. In the case of MLR modeling, the coefficient of determination (R^2) or multi-R^2 signifies how exactly fits a regression model to the training dataset. Its value close to 1 indicates a best-fitted model and vice versa [42]. The analysis of variance (ANOVA) is another check to investigate the validity of the regression model based on the hypothesis analysis. For this purpose, F-test is performed under the following hypothesis:

Null hypothesis: Dependent variable is not affected by any predictor

Alternate hypothesis: Dependent variable is affected by at least one predictor

If the probability or p-value is found less than the significance level α ($\alpha = 0.05$) the null hypothesis will be rejected and vice versa [28]. A t-test is conducted to check the validity of each predictor used in the model equation. It is also a hypothesis test for which defined null hypothesis and alternate hypothesis are as follows:

Null hypothesis: Predictors are highly dependent on one another

Alternate hypothesis: No predictor is highly dependent on other predictors

If the probability or p-value obtained from the t-test is greater than the significance level α ($\alpha = 0.05$) the null hypothesis will be accepted and vise versa. When two or more independent variables are regressed with dependent variable multicollinearity among the predictors overfits the developed model. To control this problem, the estimated value of the variance inflation factor (VIF) must be less than 10 [25]. A regression model that passes the goodness of fit test, hypothesis tests but shows a VIF value greater than 10, will not be considered as a good model.

The artificial neural network works on human brain intelligence that is analogous to the web of connected biological neurons [43]. Generally, it consists of an input layer, an output layer, and a hidden layer. A neural network may have single or multiple hidden layers between the input and output layers [44]. The hidden layer receives the input values as signals, processes them, and forwards these signals to the output layer. The neural network compares the output values with the target values and checks whether the outcomes meet the required criteria or not [45]. In the case of failure, the outcomes may be sent back for further processing and weight adjustment. In this

study, a cascade forward neural network was used which is the modified form of a feed-forward neural network. In a feed-forward neural network input layer is attached to its subsequent layers through synaptic weights. Whereas, in a cascade forward neural network an additional attachment is established between the input layer and output layer as shown in Fig. 1. This additional link ameliorates the learning rate and reduces the computational time.
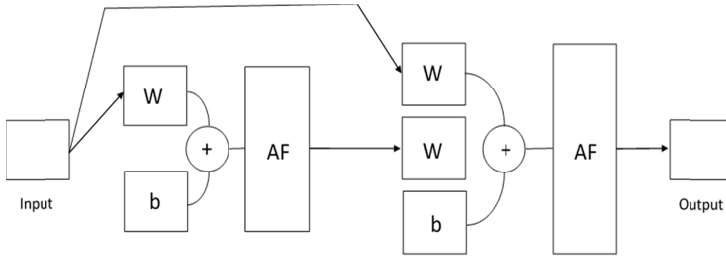

Fig. 1. The architecture of a two-layer cascade forward neural network.
Where: b, W, and AF are bias, synaptic weight, and activation function respectively

In this study, predictive relationships were developed between dynamic and physical characteristics of selected sandstones deteriorated by wetting-drying cycles. The dynamic elastic modulus and Q-factor were used as dependent variables while density, porosity, permeability, and water absorption were taken into account as independent variables.

4. Results and discussions

4.1. Effect of W-D cycles on the physico-dynamic characteristics

The effect of W-D cycles on the density of sandstone specimens is shown in Fig. 2(a). It was observed that the density of tested samples of sandstone decreased with an increase in the number of W-D cycles. The density of sandstone samples collected from the Chingi formation was highest at the 0th cycle (2654.16 kg/m^3) followed by Warcha (2595.75 kg/m^3), Tobra (2539.81 kg/m^3), Kussak (2517.87 kg/m^3), and Khewra (2356.96 kg/m^3). At the 25th cycle, the density of Khewra, Kussak, Tobra, Warcha, and Chingi Formations decreased by 3.2%, 4.2%, 3.1%, 3.2%, and 3.4% respectively (Fig. 2(b)). A similar trend of decrease in density with an increase in the number of W-D cycles was observed in previous studies [11,46]. The change in density is the result of the development of micro-cracks in the rock matrix.

An increase was found in the porosity of sandstones with the increasing W-D cycles as shown in Fig. 3(a). The porosity of the sandstone sample for Khewra formation was highest at the 0th cycle (6.37%), followed by Kussak formation (5.31%), Chingi formation (3.19%), Warcha formation (3.15%), and Tobra formation (2.07%). The percentage increase in porosity is shown in Fig. 3(b). The porosity values of Khewra, Kussak, Tobra, Warcha, and Chingi formations increased by 40.01%, 28.53%, 50.12%, 41.88%, and 24.94% respectively after 25 W-D cycles. The results were consistent with literature that explained the increase in porosity as a result of microcracks development [12].
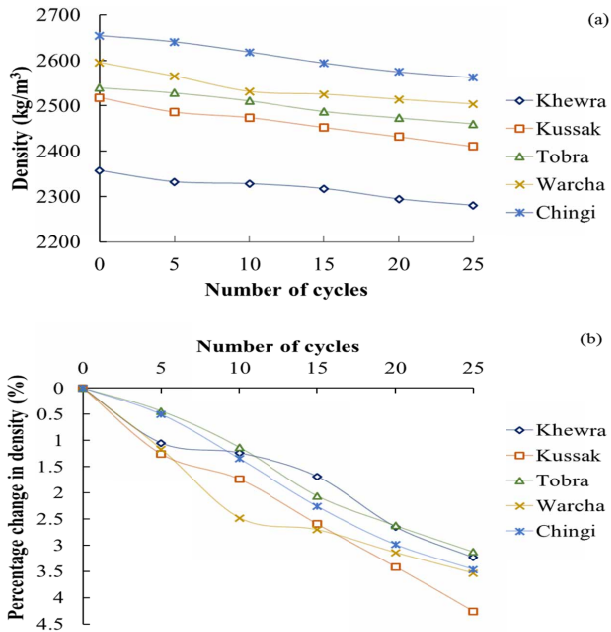
Fig. 2. The effects of W-D cycles on (a) density and (b) percentage change in density of the tested sandstone samples
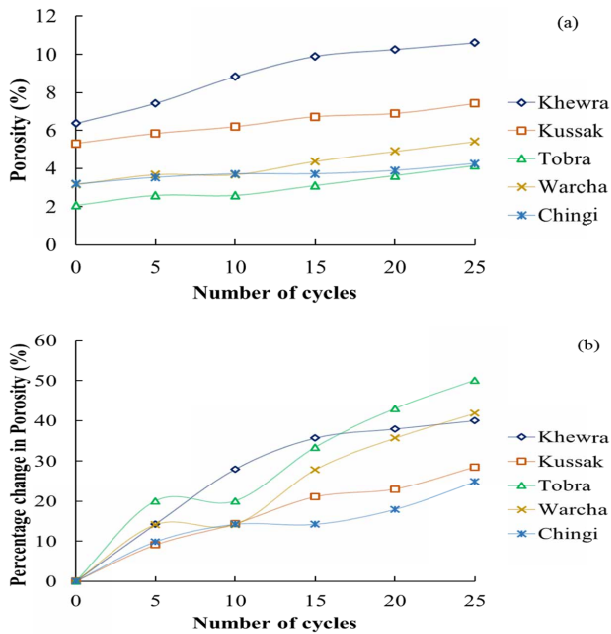

Fig. 3. The effects of W-D cycles on (a) porosity and (b) percentage change in the porosity of the tested sandstone samples

Fig. 4(a) shows the change in water absorption against W-D cycles. It was observed that as the W-D cycles increased, water absorption also increased. The sandstone of Khewra formation showed the highest value of water absorption at the 0th cycle (2.71%), followed by sandstones of Kussak formation (2.11%), Warcha formation (1.24%), Chingi formation (1.19%), and Tobra formation (0.82%). It was observed that after 25 cycles, water absorption for Khewra, Kussak, Tobra, Warcha, and Chinigi was increased by 41.21%, 28.95%, 50.30%, 42.05%, and 25.62% respectively as shown in Fig. 4(b). Similar behavior of increase in water absorption with an increase in the number of W-D cycles was also reported in the literature [12,46]. The possible reason for such trends in the development of microcracks.
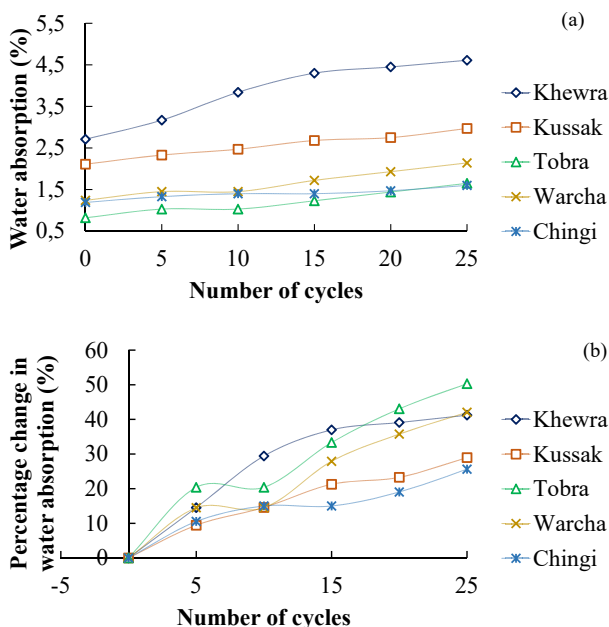

Fig. 4. The effects of W-D cycles on (a) water absorption and (b) percentage change
in water absorption of the tested sandstone samples

Fig. 5 is showing the effect of W-D cycles on the dynamic elastic Young's modulus of tested rock samples. It was observed that dynamic elastic Young's modulus decreased with an increase in the number of W-D cycles as shown in Fig. 5(a). The percentage decrease in dynamic elastic Young's modulus is shown in Fig. 5(b). It was observed that dynamic elastic Young's modulus of Khewra, Kussak, Tobra, Warcha, and Chingi formations decreased by 42.48%, 60.22%, 71.18%, 60.67%, and 49.50% respectively after 25 W-D cycles.

The effects of cyclic wetting and drying on the Q-factor is shown in Fig. 6(a). It was observed that the Q-factor decreased with an increase in the number of W-D cycles.

At the 0th W-D cycle, the highest value was observed for Tobra formation followed by Chingi, Kussak, Warcha, and Khewra formations. The values decreased gradually to the 10th cycle. After the 10th cycle, there was no major difference in the values of Q-factor amongst the
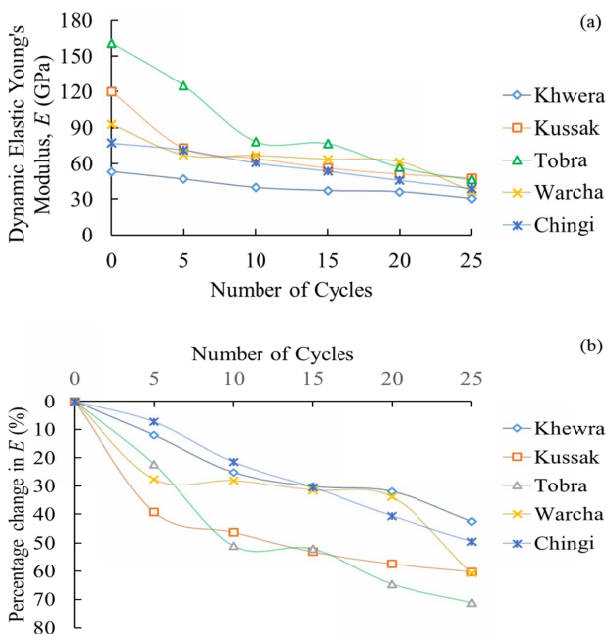
Fig. 5. The effects of W-D cycles on (a) dynamic elastic Young's modulus and (b) percentage change in dynamic elastic Young's modulus of the tested sandstone samples
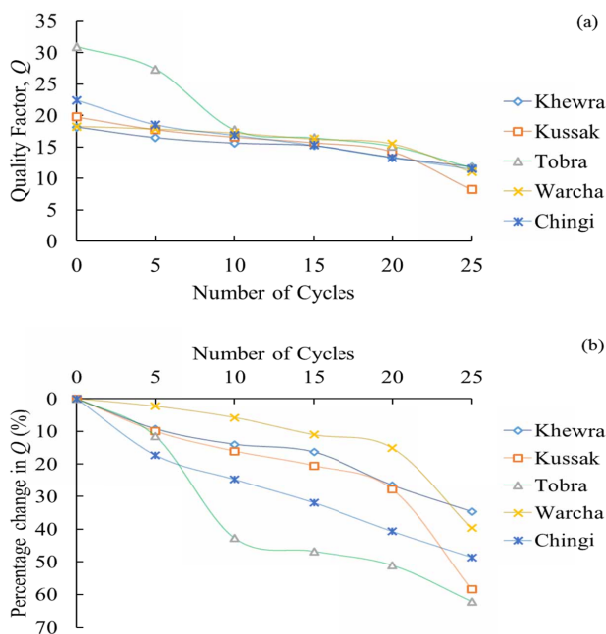

Fig. 6. The effects of W-D cycles on (a) Q-factor, and (b) percentage change in Q-factor, of the tested sandstone samples

646

tested sandstone samples. The percentage decrease in Q-factor was highest for samples of Tobra formation 62.14%, followed by Kussak 58.40%, Chingi 48.61%, Warcha 39.66%, and Khewra 34.46%. (Fig. 6(b)).

The results of E and Q-factor reveal that these observations give a better idea about the change in the rock looseness and compactness after W-D cycles. Rock is the aggregate of different minerals and each mineral has a different value of resistance to water. By increasing W-D cycles, minerals start to develop micro-cracks in their matrix material [47]. Thus, the network of micro-fractures deteriorates and exploits rock material. A rock sample free from major discontinuities may possess hidden micro flaws. In this regard, the variation in the Q-factor value provides a better understanding of the physical condition of rock.

Fig. 7 shows the change in permeability due to W-D cycles for the tested rock samples. It was observed that permeability increased with the increasing number of W-D cycles as shown in Fig. 7(a). The sandstone of Khewra formation showed the highest value of permeability at 0th cycle (2.41×10^{-7} cm/s) followed by the sandstone of Chingi formation ($1.17\times^{-7}$ cm/s), Warcha formation ($2.10\times^{-8}$ cm/s), Tobra formation ($1.27\times^{-8}$ cm/s), and Kussak formation ($1.59\times^{-8}$ cm/s). The percentage change in permeability is shown in Fig. 7(b). It was observed that as the number of W-D cycles increased, permeability also increased. Permeability of Khewra, Kussak, Tobra, Warcha, and Chingi increased by 40.01%, 28.53%, 50.12%, 41.88%, and 24.94% respectively after 25 W-D cycles.

Uniaxial compressive strength tests were performed on all the rock samples at the 0th and 25th cycles. Wetting and drying (W-D) cycles were found to affect rock strength significantly as shown in Fig. 8. At the 0th W-D cycle, Tobra formation showed the highest strength (109.7 MPa)
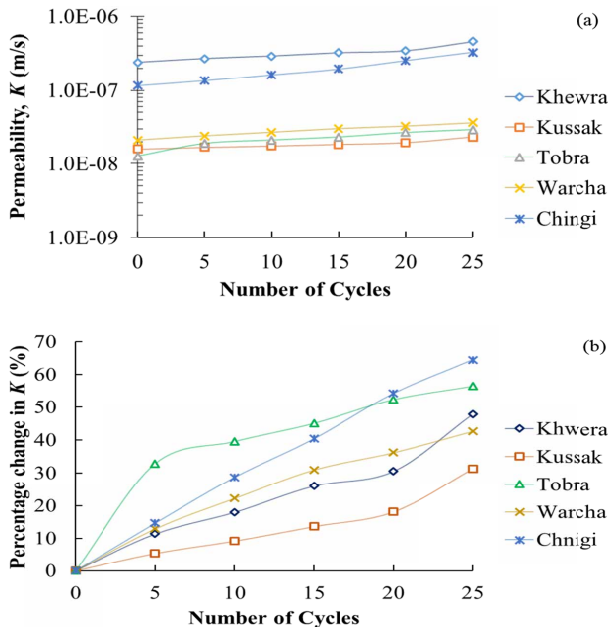

Fig. 7. The effects of W-D cycles on (a) permeability and (b) the percentage change in permeability of the tested sandstone samples

followed by Chingi formation (75.4 MPa), Kussak formation (69MPa), Warcha formation (56.8 MPa), and Khewra formation (41.6 MPa). After 25 W-D cycles, the UCS of Khewra, Kussak, Tobra, Warcha, and Chingi formations decreased by 26.97%, 42.24%, 70.09%, 46.37%, and 54.48% respectively.

The mineralogical composition of all samples was studied using thin-section microscopy. The mineral composition at the 0th and 25th cycles is shown in Table 2. No significant change in mineralogical composition was observed. The results indicate that the dissolution of minerals did not occur during W-D cycles. The resistance to the dissolution of the minerals or slaking was due to their high value of EQC. Therefore, the observed changes in the tested properties of the sandstone samples were solely due to the development of microcracks in the rock matrix undergoing repeated wetting and drying.
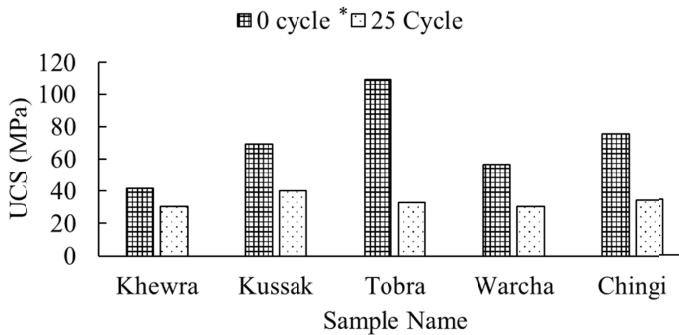

Fig. 8. The effect of W-D cycles on the UCS of tested sandstone samples

TABLE 2

Mineral composition of selected sandstone samples

Formation	Quartz		Feldspar		Clay minerals		lithic Fragment		Iron Oxide		Mica		Calcite		EQC (%)	
Cycles	0*	25	0*	25	0*	25	0*	25	0*	25	0*	25	0*	25	0*	25
Khewra	67	69	20	18	10	8	—	—	1	1	1.5	2	—	—	78	76
Kussak	78	75	17	14	0.5	1	—	—	0.5	2	4	6	—	—	84	82
Tobra	70.1	69	1.7	3	1	1	23.9	21	0.4	1	1	2	1.1	3	90	71
Warcha	56	55	28	23	9	8	3	5	3	6	1	2	—	—	68	68
Chingi	63	59	7	7	—	—	18	22	—	—	—	—	12	12	65	61

* Bakar et al. [51].

4.2. Statistical data modelling

Table 3 shows the results of bivariate analysis between the measured dynamic-physical properties of sandstones. The values of one-to-one relationships between the parameters are followed by the superscript single steric (*) and double steric (**) that indicates significant correlations at the confidence interval (*CI*) level of 95% and 99% respectively. Results show that among all relationships between physical properties, Density vs Porosity ($R = -0.87$), Density

vs Water Absorption ($R = -0.89$), and Porosity vs Water Absorption ($R = 0.99$) had the highest values of R at the *CI* level of 99%. Similarly, the relationship between the dynamic properties Q-factor vs Elastic modulus ($R = 0.88$) was found significant at the *CI* level of 99%. Before conducting the regression analysis, the bivariate analysis helps to identify the variable that may produce multicollinearity.

In this analysis, Elastic modulus and Q-factor were regressed with the density, porosity, permeability, and water absorption using the stepwise method. In this method, the numbers of variables are increased in the model equation step-by-step to get significant prediction models. A regression model is said to be significant if it has a high value of multi-R^2, VIF value less than 10 and validated by hypothesis testing. Table 4 and Table 5 demonstrate the R^2-statistics of the generated models. In the first step, the Q-factor was regressed with the porosity only, and in the second step, it made a relationship between porosity and water absorption. The multi-R^2 improves as the numbers of predictors are increased in the model equation [26]. As shown in Table 4, the R^2 for model-1 was recorded as 0.24. In the case of model-2, two variables were regressed with the dependent variable therefore, its R^2 value (i.e. 0.45) was found greater than model-1. In the case of elastic modulus (E), only porosity was able to make a correlation with E. Its R^2 value was estimated as 0.36 (see Table 5).

TABLE 3

Bivariate analysis between the measured parameters

		Density	Porosity	Water Absorption	Permeability	Q-factor	Elastic Modulus
Density	Pearson Correlation	1					
	Sig. (2-tailed)						
Porosity	Pearson Correlation	-0.87^{**}	1				
	Sig. (2-tailed)	0.00					
Water Absorption	Pearson Correlation	-0.89^{**}	0.99^{**}	1			
	Sig. (2-tailed)	0.00	0.00				
Permeability	Pearson Correlation	-0.49^{**}	0.61^{**}	0.63^{**}	1		
	Sig. (2-tailed)	0.00	0.00	0.00			
Q-factor	Pearson Correlation	0.36	-0.49^{**}	-0.46^{*}	-0.31	1	
	Sig. (2-tailed)	0.05	0.00	0.01	0.09		
Elastic Modulus	Pearson Correlation	0.45^{*}	-0.60^{**}	-0.58^{**}	-0.54^{**}	0.88^{**}	1
	Sig. (2-tailed)	0.01	0.00	0.00	0.00	0.00	
** Correlation is significant at the 0.01 level (2-tailed)							
* Correlation is significant at the 0.05 level (2-tailed)							

Table 6 and Table 7 display the results of the ANOVA test. For Q-factor, the probability value of both model-1 and model-2 was found less than the significance level $\alpha = 0.05$. This signifies that both models had rejected the null hypothesis (i.e. Dependent variable is not affected by

R^2-statistics for the prediction models

Model	R	R Square	Adjusted R Square	Std. Error of the Estimate
1	0.49[a]	0.24	0.22	3.98
2	0.67[b]	0.45	0.41	3.47
a – Predictors: (Constant), Porosity with Dependent variable (Q-factor)				
b – Predictors: (Constant), Porosity, Water Absorption with Dependent variable (Q-factor)				

R^2-statistics for the prediction models

Model	R	R Square	Adjusted R Square	Std. Error of the Estimate
1	0.60[a]	0.36	0.34	23.51
a – Predictors: (Constant), Porosity with Dependent variable (E)				

any predictor) as described in Table 6. In the case of elastic modulus, the developed regression model also accepted the alternate hypothesis (see Table 7). Since all models have rejected the null hypothesis therefore F-test has validated alternate hypothesis.

Results of the ANOVA test to check the significance of regression models

Model[a]		Sum of Squares	df[d]	Mean Square	F[e]	Sig. [f]
1	Regression	144.59	1	144.59	9.08	0.00[b]
	Residual	445.73	28	15.92		
	Total	590.32	29			
2	Regression	265.11	2	132.55	11.00	0.00[c]
	Residual	325.22	27	12.04		
	Total	590.32	29			
a – Dependent Variable: Q-factor						
b – Predictors: (Constant), Porosity						
c – Predictors: (Constant), Porosity, Water Absorption						
d – Degree of freedom						
e – Mean square ratio						
f – Significance value						

Results of the ANOVA test to check the significance of regression models

Model[a]		Sum of Squares	df[c]	Mean Square	F[d]	Sig.[e]
1	Regression	8704.62	1	8704.62	15.74	0.00[b]
	Residual	15481.38	28	552.91		
	Total	24186.01	29			
a – Dependent Variable: Elastic modulus (E)						
b – Predictors: (Constant), Porosity						
c – Degree of freedom						
d – Mean square ratio						
e – Significance value						

After the F-test analysis, the t-test was applied to check the validity of each predictor used in the model equation. Table 8 illustrates that for Q-factor the value of significance level ($\alpha = 0.05$) of both model-1 and model-2 was determined greater than the probability value obtained from the t-test analysis. Therefore, both models accepted the alternate hypothesis (No predictor is highly dependent on other predictors). The collinearity statistics show that the VIF value for model-1 was estimated as 1. However, in the case of model-2, the VIF value was found far greater than the threshold limit (VIF = 211.15 > 10). Thus, model-2 cannot be accepted due to its high multicollinearity problem. For elastic modulus (E), the probability value of the predictor in the model equation was found less than the significance level ($\alpha = 0.05$) as demonstrated in Table 9. In this case, E made a relationship with only a single predictor (i.e. porosity) and its VIF value was determined as 1. Therefore, no multicollinearity problem arose. The final prediction model equations for the estimation of Q-factor and elastic modulus are as follows:

$$Q\text{-factor} = 21.49 - 0.94\Phi \tag{6}$$

$$E = 102.97 - 7.30\Phi \tag{7}$$

TABLE 8

The t-test results along with collinearity statistics

Model[a]		Unstandardized Coefficients		Standardized Coefficients	t [b]	Sig. [c]	95.0% Confidence Interval for B		Collinearity Statistics	
		B	Std. Error	Beta			Lower Bound	Upper Bound	Tolerance	VIF
1	(Constant)	21.49	1.79		11.99	0.0	17.82	25.17		
	Porosity	−0.94	0.31	−0.49	−3.01	0.0	-1.58	-0.301	1.00	1.00
2	(Constant)	27.72	2.51		11.04	0.0	22.57	32.87		
	Porosity	−13.39	3.94	−7.04	−3.39	0.0	-21.49	-5.29	0.00	211.15
	Water Absorption	27.76	8.78	6.56	3.16	0.0	9.75	45.77	0.00	211.15
a – Dependent Variable: Q-factor										
b – t-test score										
c – Significance value										

TABLE 9

The t-test results along with collinearity statistics

Model[a]		Unstandardized Coefficients		Standardized Coefficients	t [b]	Sig. [c]	95.0% Confidence Interval for B		Collinearity Statistics	
		B	Std. Error	Beta			Lower Bound	Upper Bound	Tolerance	VIF
1	(Constant)	102.97	10.57		9.74	0.00	81.32	124.62		
	Porosity	−7.30	1.84	−0.60	−3.97	0.00	−11.07	−3.53	1.00	1.00
a – Dependent Variable: Elastic modulus (E)										
b – t-test score										
c – Significance value										

The validation of Eq. (5) and Eq. (6) was done using a separate dataset of the physical and dynamic properties of the sandstones deteriorated by wetting-drying cycles. Fig. 9(a-b) illustrate the relationship between the estimated and predicted values of Q-factor and E respectively in terms of their goodness of fit (R^2). The R^2 value for Q-factor and E was determined as 0.30 and 0.36 respectively. This indicates that both models are not good enough for the estimation of Q-factor and E.
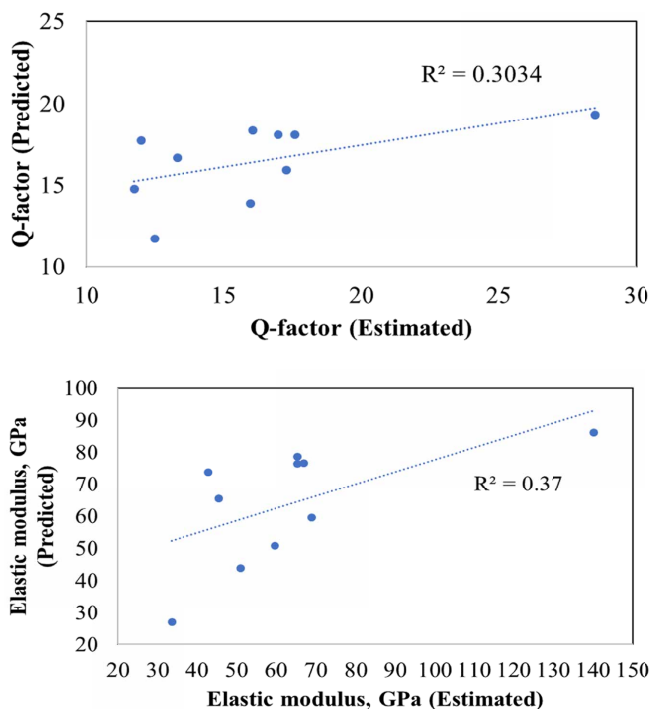

Fig. 9. The scatter plot between the estimated and predicted values of the (a) Q-factor and (b) elastic modulus (E) through the multiple linear regression analysis

It is evident from the results of multivariate statistics that no multiple linear regression model was developed between the physical and dynamic properties of the sandstones. A high level of multicollinearity restricted the prediction models to only one-to-one relationships with a low value of goodness of fit. To overcome this problem, a backpropagation neural network technique i.e. cascade-forward neural network was used to train prediction models. The training of a neural network is an adaptive process that gives different outcomes for each attempt. This process continues until the output values come up very close to the target values. Fig. 10a shows the mean squared error (MSE) plot for Q-factor to find the MSE between the training, validation, and test values. The best validation performance was 8.38 in terms of MSE at cycle 1. In the case of elastic modulus, the minimum value of MSE between the training, validation, and test values, was recorded as 298.8 at cycle 1. After that error values were started to increase as shown in Fig. 10b.
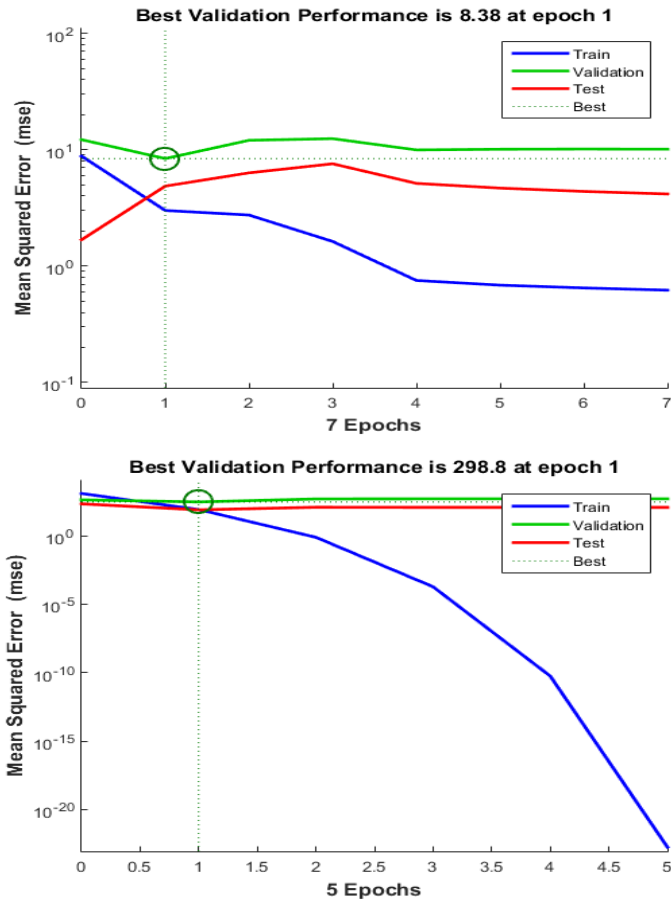
Fig. 10. The mean squared error convergence between training, validation,
and test values for the (a) Q-factor and (b) elastic modulus (E)

The training and learning phase help to fit the model on the training dataset by evaluating the relationship between the output values and target values as described in Fig. 11 and Fig. 12 for both Q-factor and E respectively. In the case of the Q-factor the Pearson's correlation (R) for training, validation, and testing was determined as 0.93, 0.88, and 0.90 respectively. The overall R-value for dependent variable E was found as 0.92. Furthermore, the relationship (R-value) between the output and target values during training, validation, and testing was estimated as 0.95, 0.89, and 0.87 respectively as demonstrated in Fig. 12.

The prediction models developed by the neural network were validated by using a separate validation dataset. The goodness of fit or coefficient of determination (R^2) between the estimated and predicted values for Q-factor and E was calculated as 0.86 and 0.91 respectively (see Fig. 13(a-b)). These results are much better than those determined by the multiple linear regression analysis. It shows that in prediction modeling, the neural network has a competitive edge over linear regression analysis. Because in linear regression, the ordinary least-squaring method
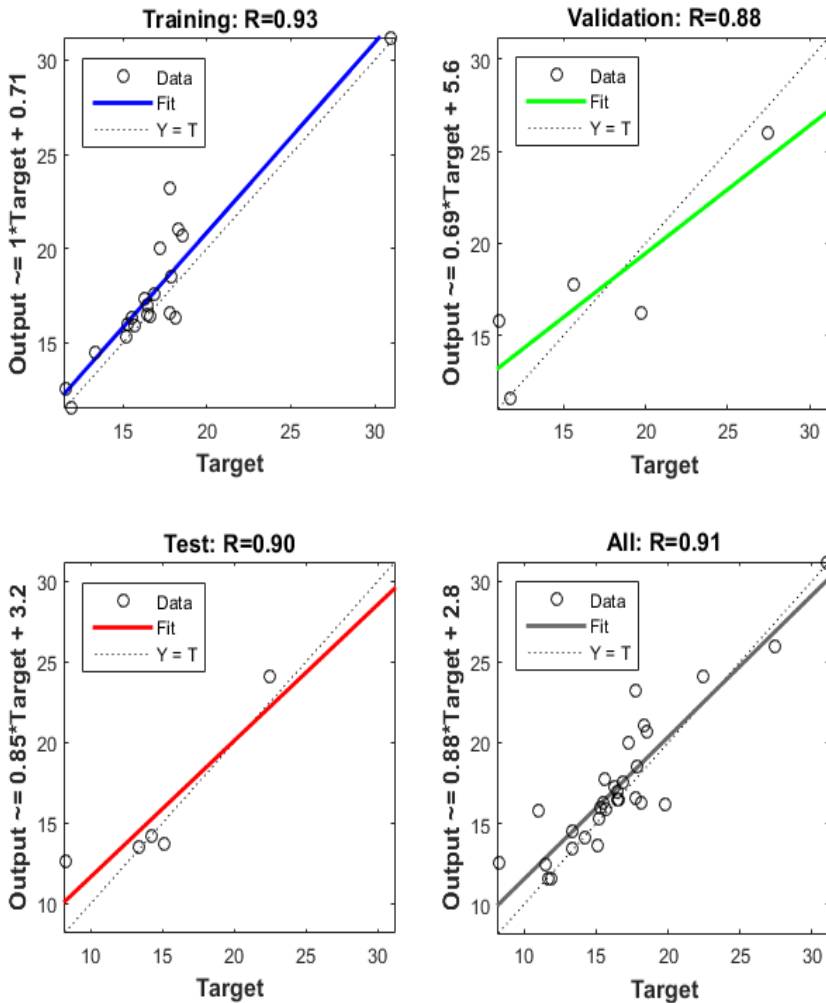
Fig. 11. Pearson's correlation (R) between the output and target values of dependent variable Q-factor during the training, validation, and testing of the dataset

and multicollinearity restrict to have significant models. Whereas, in the neural network, the optimization of configured models and fitting of nonlinear function to training dataset enhances their performance.

5. Conclusion

This research work focuses to study the effect of W-D cycles on the physico-dynamic properties of sandstones taken from the salt range area of Pakistan. For this purpose, a series of laboratory tests were performed to investigate any significant change in the engineering properties of the
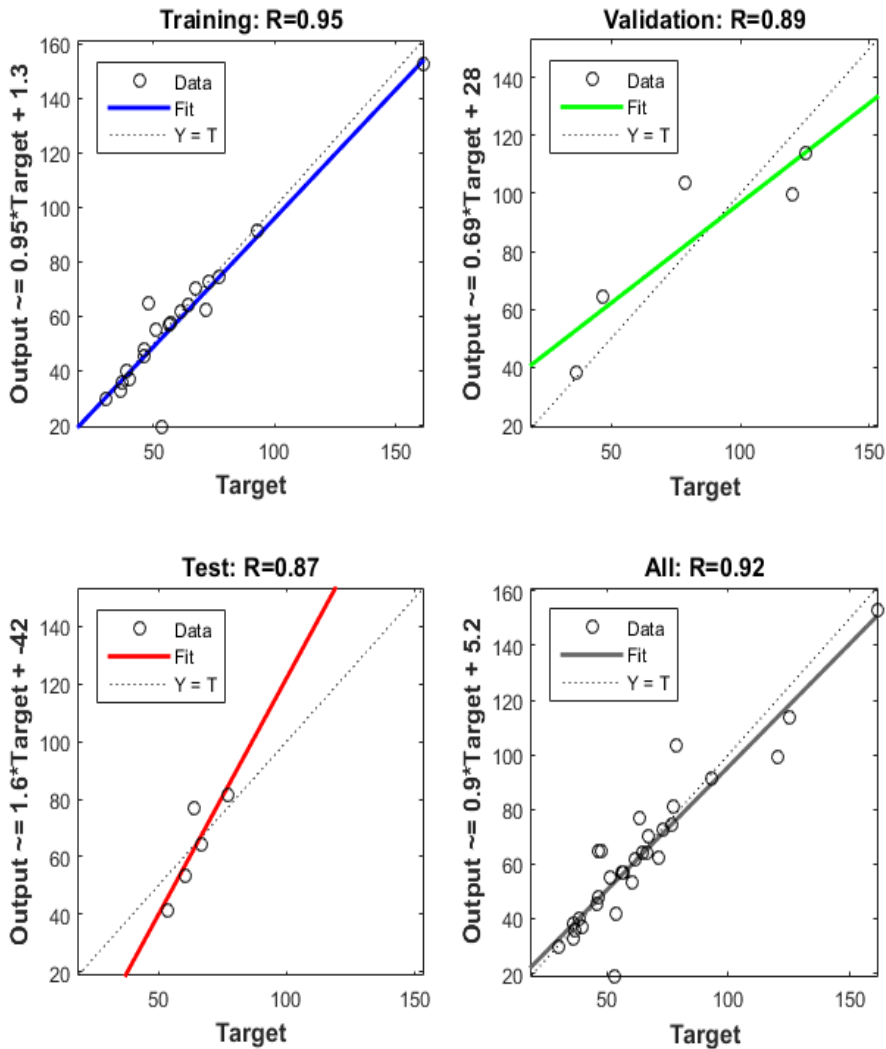
Fig. 12. Pearson's correlation (R) between the output and target values of dependent variable E during the training, validation, and testing of the dataset

sandstones in terms of their density, porosity, permeability, water absorption, Q-factor, elastic modulus, and unconfined compressive strength (UCS). Results show that with the increase in the number of W-D cycles, the measured values of density, Q-factor, and elastic modulus depreciate. Whereas, the estimated values of porosity, permeability, and water absorption appreciate. The overall maximum reduction in density, Q-factor, and elastic modulus was found as 3-4%, 34-62%, and 42-71% respectively. In the case of porosity, permeability, and water absorption, the maximum increment was determined as 24-50%, 31-64%, and 25-50% respectively. The development of intergranular cracking in rocks deteriorated by the wetting-drying cycles leads to a reduction
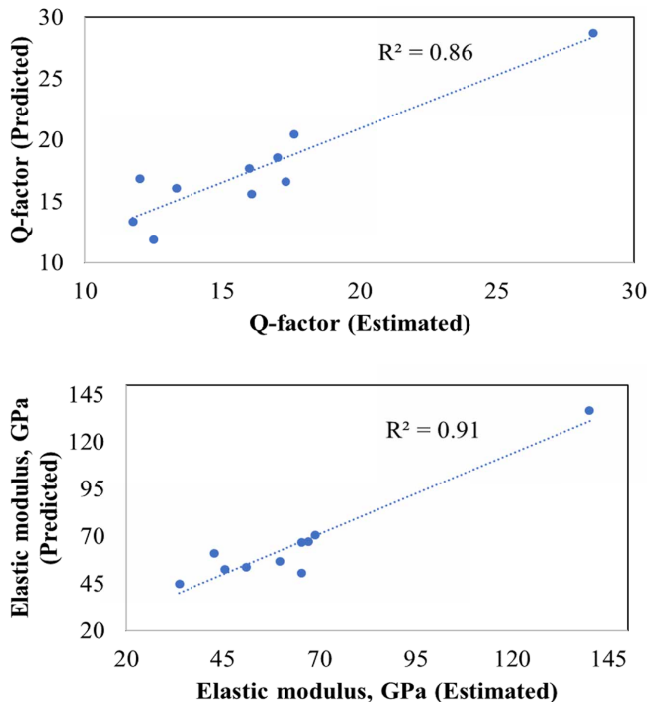
Fig. 13. The scatter plot between the estimated and predicted values of the (a) Q-factor and (b) elastic modulus (E) through the cascade-forward neural network

in their strength. This fact was studied by conducting a UCS test on sandstone samples treated under wetting-drying cycles. Their UCS values got reduced by 26-70%.

After evaluating the effects of W-D cycles on the physical and dynamic properties of the sandstone samples, bivariate analysis was performed to identify the variables having strong correlations. The physical parameters, density, porosity, and water absorption showed a strong correlation with one another. Their Pearson's coefficient (R) values ranged from 0.87-0.99. In the case of dynamic parameters, Q-factor, and elastic modulus made a good relationship with each other ($R = 0.88$).

To make an empirical relationship between the dynamic and physical properties of the tested sandstone samples regression analysis was performed using the stepwise method. Two regression models were developed using Q-factor as a dependent variable with R^2 values of 0.24 and 0.45 respectively. Both models were found significant in their hypothesis testing; however, the VIF value for model-2 was found much greater than the threshold limit. Therefore, only model-1 was considered significant. In the case of elastic modulus (E), only porosity was regressed with the dependent variable E, and the rest of the predictors were excluded from analysis due to their high multicollinearity problem.

The validation of the developed linear regression models was done using a validation dataset. The value of R^2 between the estimated and predicted values of Q-factor and E was determined as 0.30 and 0.36 respectively. The linear regression analysis did not provide satisfactory results.

656

Therefore, the cascade-forward neural network technique was employed to develop meaningful prediction models. The neural network fitted the nonlinear function to the training dataset and optimized it as well to get the optimal solution. The best validation performance was noted at cycle 1 for both Q-factor and E. At cycle 1 the mean squared error (MSE) for Q-factor and E was estimated by 8.38 and 298.8 respectively. During the training, validation, and testing the overall relationship (R-value) between the output and the target value for Q-factor and E was calculated as 0.91 and 0.92 respectively. The validation of prediction models generated by the neural network showed that they had a high value of goodness of fit. The R^2 between the estimated and predicted values of Q-factor and E were found as 0.86 and 0.91 respectively.

The overall results of this research work reveal the significance of W-D cycles as a major factor that alters the dynamic and physical properties of the rocks. Such studies are of utmost importance for the local areas to better understand the engineering behavior of the rocks undergoing environmental changes during and after the construction of mega structures.

Declaration of Conflict of Interest

On the behave of all co-authors, the corresponding author declares that there is no potential conflict of interest regarding this manuscript.

Reference

[1] Wu. Faquan, Qi. Shengwen, Lan. Hengxing, Mechanism of uplift deformation of the dam foundation of Jiangya Water Power Station, Hunan Province, PR China. Hydrogeol. J. **13** (3), 451-466 (2005).

[2] O. Aydan, The inference of physico-mechanical properties of soft rocks and the evaluation of the effect of water content and weathering on their mechanical properties from needle penetration tests. In: 46th US rock mechanics/geomechanics symposium, American Rock Mechanics Association (2012).

[3] M. Duda, J. Renner, The weakening effect of water on the brittle failure strength of sandstone. Geophys. J. Int. **192** (3), 1091-1108 (2013).

[4] P.L.P. Wasantha, P.G. Ranjith, Water-weakening behavior of Hawkesbury sandstone in brittle regime. Eng. Geol. **178**, 91-101 (2014).

[5] F. Cherblan, J. Berthonneau, P. Bromblet, V. Huon, Influence of water content on the mechanical behaviour of limestone: Role of the clay minerals content. Rock Mech. Rock Eng. **49** (6), 2033-2042 (2016).

[6] M.R. Vergara, T. Triantafyllidis, Influence of water content on the mechanical properties of an argillaceous swelling rock. Rock Mech. Rock Eng. **49** (7), 2555-2568 (2016).

[7] C. Gökceoğlu, R. Ulusay, H. Sönmez, Factors affecting the durability of selected weak and clay-bearing rocks from Turkey, with particular emphasis on the influence of the number of drying and wetting cycles. Eng. Geol. **57** (3-4), 215-237 (2000).

[8] N. Reviron, T. Reuschlé, J.D. Bernard, The brittle deformation regime of water-saturated siliceous sandstones. Geophys. J. Int. **178** (3), 1766-1778 (2009).

[9] W. He, K. Chen, A. Hayatdavoudi, K. Sawant, M. Lomas, Effects of clay content, cement and mineral composition characteristics on sandstone rock strength and deformability behaviors. J. Pet. Sci. Eng. **176**, 962-969 (2019).

[10] P.D. Sumner, M.J. Loubser, Experimental sandstone weathering using different wetting and drying moisture amplitudes. Earth. Surf. Process. Landf. **33** (6), 985-990 (2008).

[11] A. Özbek, Investigation of the effects of wetting-drying and freezing-thawing cycles on some physical and mechanical properties of selected ignimbrites. Bull. Eng. Geol. Environ. **73** (2), 595-609 (2014).

[12] G. Khanlari, Y. Abdilor, Influence of wet-dry, freeze-thaw, and heat-cool cycles on the physical and mechanical properties of Upper Red sandstones in central Iran. Bull. Eng. Geol. Environ. **74** (4), 1287-1300 (2015).

[13] H. Deng, J. Li, M. Zhu, K.W. Wang, L.H. Wang, C.J. Deng, Experimental research on strength deterioration rules of sandstone under "saturation-air dry" circulation function. Rock Soil Mech. **33** (11), 3306-3312 (2012).

[14] P.A. Hale, A. Shakoor, A laboratory investigation of the effects of cyclic heating and cooling, wetting and drying, and freezing and thawing on the compressive strength of selected sandstones. Environ. Eng. Geosci. **9** (2), 117-130 (2003).

[15] B.Y. Zhang, J.H. Zhang, G.L. Sun, Deformation and shear strength of rockfill materials composed of soft siltstones subjected to stress, cyclical drying/wetting and temperature variations. Eng. Geol. **190**, 87-97 (2015).

[16] W. Hua, S. Dong, Y. Li, J. Xu, Q. Wang, The influence of cyclic wetting and drying on the fracture toughness of sandstone. Int. J. Rock Mech. Min. Sci. **100** (78), 331-335 (2015).

[17] X. Liu, Z. Wang, Y. Fu, W. Yuan, L. Miao, Macro/microtesting and damage and degradation of sandstones under dry-wet cycles. Adv. Mater. Sci. Eng. (2016).

[18] A.V. Turkington, T.R. Paradise, Sandstone weathering: a century of research and innovation. Geomorphology **67** (1-2), 229-253 (2005).

[19] G. Andriani, N. Walsh, Fabric, porosity and water permeability of calcarenites from Apulia (SE Italy) used as building and ornamental stone. Bull. Eng. Geol. Environ. **62** (1), 77-84 (2003).

[20] B. Fitzner, R. Kownatzki, Porositätseigenschaften und Verwitterungsverhalten von sedimentären Naturwerksteinen. Ernst & Sohn, (1991).

[21] M.M. Demarco, E. Jahns, J. Rudrich, P. Oyhantcabal, S. Siegesmund, The impact of partial water saturation on rock strength: an experimental study on sandstone. Zeitschrift der Deutschen Gesellschaft fur Geowissenschaften, **158** (4), 869 (2007).

[22] E.A. Eissa, A. Kazi, Relation between static and dynamic Young's moduli of rocks. Int. J. Rock Mech. Min. Sci. **25** (6), (1988).

[23] S.R. Agha, M.J. Alnahhal, Neural network and multiple linear regression to predict school children dimensions for ergonomic school furniture design. Appl. Ergon. **43** (6), 979-984 (2012).

[24] M. Karakus, M. Kumral, O. Kilic, Predicting elastic properties of intact rocks from index tests using multiple regression modelling. Int. J. Rock Mech. Min. Sci. **42** (2), 323-330 (2005).

[25] M.H. Kutner, C.J. Nachtsheim, J. Neter, Simultaneous inferences and other topics in regression analysis. Applied linear regression models. 4th ed. McGraw-Hill Irwin, New York, NY, 168-170 (2007).

[26] R.S. Akan, K. Nilay, U. Soner, Multiple regression model for the prediction of unconfined compressive strength of jet grout columns. Proc. Earth Planet Sci. **15**, 299-303 (2015).

[27] M.F. Ahmed, U. Waqas, M. Arshad, J.D. Rogers, Effect of heat treatment on dynamic properties of selected rock types taken from the Salt Range in Pakistan. Arab. J. Geosci. **11** (22), 1-13 (2018).

[28] U. Waqas, M.F. Ahmed, M. Arshad, Classification of the intact carbonate and silicate rocks based on their degree of thermal cracking using discriminant analysis. Bull. Eng. Geol. Environ. 1-13 (2020).

[29] K.A. Aali, M. Parsinejad, B. Rahmani, Estimation of Saturation Percentage of Soil Using Multiple Regression, ANN, and ANFIS Techniques. Comput. Info. Sci. **2** (3), 127-136 (2009).

[30] A.A.K. Ghauri, A preliminary account of the texture, structure and mineralogy composition of the Khewra formation, CIS Indus salt range, west Pakistan. J. Himal. Earth Sci. **5**, (1970).

[31] M. Jehangiri, M. Hanif, M. Arif, I.U. Jan, S. Ahmad, The Early Cambrian Khewra Sandstone, Salt Range, Pakistan: endorsing southern Indian provenance. Arab. J. Geosci. **8** (8), 6169-6187 (2015).

[32] S. Khan, M.M. Shah, Multiphase dolomitization in the Jutana Formation (Cambrian), Salt Range (Pakistan): Evidences from field observations, microscopic studies and isotopic analysis. Geologica Acta **17**, 1-18 (2019).

[33] S.M.I. Shah, Stratigraphy of Pakistan; Government of Pakistan. Ministry of Petroleum and Natural Resources. Geological Survey of Pakistan (2009).

[34] ISRM, Suggested methods for rock characterization, testing, and monitoring: 2007-2014. Springer (2007).

[35] US Army Corps of Engineers, (2012) http://gsl.erdc.usace.army.mil/SL/MTC/hand book/RT/RTH/116-95.pdf

[36] P.B. Kurt-Karakus, T.F. Bidleman, K.C. Jones, Chiral organochlorine pesticide signatures in global background soils. Environ. Sci. Technol. **39** (22), 8671-8677 (2005).

[37] J.A. Franklin, Suggest methods for determining water content, porosity, density, absorption and related properties and swelling and slake-durability index properties. Int. J. Rock Mech. Min. Sci. & Geomech. Abstr. **16**, 141-156 (1979).

658

[38]   S.L. Kramer, Geotechnical earthquake engineering. Pearson Education India (1996).

[39]   ASTM C-215-91, Standard Test Method for Fundamental Transverse, Longitudinal, and Torsional Frequencies of Concrete Specimens (2003).

[40]   ASTM D-2938-9, Standard Test Method for Unconfined Compressive Strength of Intact Rock Core Specimens (1992).

[41]   J. Schimazek, H. Knatz, Der Einfluß des Gesteinsaufbaus auf die Schnittgeschwindigkeit und den Meißelverschleiß von Streckenvortriebsmaschinen. Glückauf. **106** (6), 274-278 (1970).

[42]   Y. Abdi, A.T. Garavand, R.Z. Sahamieh, Prediction of strength parameters of sedimentary rocks using artificial neural networks and regression analysis. Arab. J. Geosci. **11** (19), 1-11 (2018).

[43]   E.T. Mohamad, D.J. Armaghani, E. Momeni, A.H. Yazdavar, M. Ebrahimi, Rock strength estimation: a PSO-based BP approach. Neural. Comput. Appl. **30** (5), 1635-1646 (2018).

[44]   M. Khandelwal, T.N. Singh, Predicting elastic properties of schistose rocks from unconfined strength using intelligent approach. Arab. J. Geosci. **4** (3-4), 435-442 (2011).

[45]   B.R. Kumar, H. Vardhan, M. Govindaraj, S.P. Saraswathi, Artificial neural network model for prediction of rock properties from sound level produced during drilling. Geomech. Geoeng. **8** (1), 53-61 (2013).

[46]   Z. Zhou, X. Cai, L. Chen, W. Cao, Y. Zhao, C. Xiong, Influence of cyclic wetting and drying on physical and dynamic compressive properties of sandstone. Eng. Geol. **220**, 1-12 (2017).

[47]   S. Chaki, M. Takarli, W.P. Agbodjan, Influence of thermal damage on physical properties of a granite rock: porosity, permeability and ultrasonic wave evolutions. Constr. Build. Mater. **22** (7), 1456-1461 (2008).

[48]   B. Vàsàrhelyi, P. Vàn, Influence of water content on the strength of rock. Eng. Geol. **84**, 70-74 (2006).

[49]   P. Malkowski, L. Ostrowski, P. Bozecki, The impact of the mineral composition of Carboniferous claystones on the water-induced changes of their geomechanical properties. Geol. Geophys. Environ. **43** (1), 43-55 (2017).

[50]   U. Waqas, M.F. Ahmed, Prediction Modeling for the Estimation of Dynamic Elastic Young's Modulus of Thermally Treated Sedimentary Rocks Using Linear-Nonlinear Regression Analysis, Regularization, and ANFIS. Rock Mech. Rock Eng. **53** (12), 5411-5428 (2020).

[51]   M.A. Bakar, Y. Majeed, J. Rostami, Effects of rock water content on CERCHAR Abrasivity Index. Wear **368**, 132-145 (2016).